European Polymer Journal 258 (2026) 115076

Contents lists available at ScienceDirect

European Polymer Journal

journal homepage: www.elsevier.com/locate/europolj

Recombinant antimicrobial mussel adhesive protein-integrated PVA nanofibers with stable and long-lasting antibacterial activity

Daun Lim [a,b,c,1], Young Nam Kim [a,1], Kundan Singh Rawat [a,1], Won-Hui Jeong [a,h], Somi Yoon [a,d], Jeong Jae Wie [d,e,f], Eun-Bin Chu [g], Yong-Tae Kim [g], Yoong Ahm Kim [b,*], Yong Chae Jung [a,*]

[a] Convergence Research Center for Recyclable Air Mobility Materials and Platform, Korea Institute of Science and Technology (KIST), 92 Chudong-ro, Bongdong-eup, Wanju-gun, Jeonbuk 55324, South Korea
[b] Department of Polymer Engineering, Graduate School, School of Polymer Science and Engineering Chonnam National University, 77 Yongbong-ro, Buk-gu, Gwangju 61186, South Korea
[c] DH AUTONEX, 55 Yongji-ro, Yongji-myeon, Gimje-si, Jeonbuk 54336, South Korea
[d] Department of Organic and Nano Engineering, Hanyang University, 222 Wangsimni-ro, Seongdong-gu, Seoul 04763, South Korea
[e] Human-Tech Convergence Program, Hanyang University, 222 Wangsimni-ro, Seongdong-gu, Seoul 04763, South Korea
[f] Department of Chemical Engineering, State University of New York College of Environmental Science and Forestry, 1 Forestry Drive, Syracuse, NY 13210, USA
[g] BIOVIT 30, Beotkkot-ro 36-gil, Geumcheon-gu, Seoul 08511, South Korea
[h] Department of Nano Convergence Engineering, Jeonbuk National University, Jeonju-si 54896, Jeonbuk-do, South Korea

ARTICLE INFO

Keywords:
Recombinant antimicrobial mussel adhesive protein
Adhesive protein
Nanofiber
Antimicrobial
PVA

ABSTRACT

Conventional antibacterial systems often suffer from limited durability due to the leaching of active components and concerns associated with the inorganic antibacterial agents. Hence, there is growing interest in developing advanced antibacterial platforms that can integrate surface functionality, non-antibiotic mechanisms, and the long-term stability. Herein, we report recombinant antimicrobial mussel adhesive protein (AMAP) was incorporated into a poly(vinyl alcohol) (PVA) matrix, and electrospun to form nanofiber webs with an average diameter of ~ 330 nm. The as-spun nanofibers were subsequently rendered water-insoluble via thermal treatment, followed by systematic characterization of their structural evolution, surface properties, wettability, and their antibacterial performance. The AMAP-incorporated nanofibers exhibited significantly enhanced structural integrity compared to pristine PVA, maintaining their morphology even after prolonged water immersion treatment. The surface wettability underwent a pronounced transition from moderately hydrophobic (71.7°) to highly hydrophilic (16.2°) upon thermal treatment. This transition also contributed to a bacterial reduction rate of 96.0% against *S. aureus* (*S. aureus*), and 92.9% against *Escherichia coli* (*E. coli*), while retaining 91.3% and 87.5% antibacterial activity against *S. aureus* and *E. coli*, respectively, after 30 days of storage under the ambient conditions. These results demonstrate that the AMAP incorporation, combined with thermal processing, enables simultaneous structural stabilization and surface functionalization through amphiphilic intermolecular interactions with the PVA matrix, providing an effective strategy for sustained antibacterial performance without antibiotics or inorganic agents.

1. Introduction

In early 2020, the global spread of COVID-19 and the resulting full-scale pandemic fundamentally changed the awareness of microbial contamination, infection and transmission not only in medical institutions but also in daily life, including public transportation, educational facilities, and homes. In particular, as the introduction of the antibacterial coatings, antibacterial plastics, and antibacterial filters has rapidly expanded, especially for high-contact surfaces in hospitals, private institutions and public facilities, antibacterial functional materials have become one of the key infrastructures for infection control.

Over the past decade, research trends have shifted away from simply

* Corresponding authors.
E-mail addresses: yak@chonnam.ac.kr (Y.A. Kim), ycjung@kist.re.kr (Y.C. Jung).
[1] These authors contributed equally to this work.

https://doi.org/10.1016/j.eurpolymj.2026.115076
Received 16 June 2026; Received in revised form 7 September 2026; Accepted 8 September 2026
Available online 9 September 2026
0014-3057/© 2026 The Authors. Published by Elsevier Ltd. This is an open access article under the CC BY-NC-ND license (http://creativecommons.org/licenses/by-nc-nd/4.0/).

loading or releasing antibacterial agents towards approaches that simultaneously consider surface functionalization, non-antibiotic-based antibacterial materials, and the achievement of the long-term functional stability [1–3]. In particular, electrospun nanofibers have attracted significant attention as a promising material technology for a wide range of applications, including medical filters, wound dressings, protective clothing, HVAC and air purification systems, and packaging materials, due to their high specific surface area, excellent pore structure controllability, and versatile potential for chemical functionalization. Electrospinning can produce continuous fibers with diameters ranging from tens to hundreds of nanometers through a relatively simple solution process and therefore offers structural features and manufacturing advantages suitable for combining the physical capture of fine particles and microorganisms with chemically imparted antibacterial functions on the surface [2–5].

The active components used in antibacterial materials have gradually expanded beyond their initial focus on silver nanoparticles, metal oxides, antibiotics, and natural extracts. As promising alternatives to overcome the limitations of conventional materials, such as the induction of resistance, cytotoxicity, non-uniform release behavior, and long-term functional deterioration, bio-derived functional molecules such as antimicrobial peptides (AMPs) are attracting increasing attention [1,3,5]. Felgueiras et al. defined AMP-conjugated electrospun nanofibers as a promising approach that can maximize the functionality of wound healing [1], Homaeigohar et al. reported that antibacterial nanofiber dressings are expanding beyond conventional simple antibiotic-delivery systems into biohybrid platforms containing antibacterial nanoparticles, natural products, and bio-derived functional molecules [3].

Recent studies on functional fibers employing AMPs have moved beyond simple blended or release-type systems and are being developed toward the immobilization of functional proteins or peptides to substrates in order to enhance surface stability and functional persistence. Song et al. immobilized an LL37-derived peptide on the surface of silk fibroin nanofibers and reported not only antibacterial activity but also the promotion of cell proliferation, keratinocyte differentiation, and suppression of inflammatory cytokine expression [6]. Yang et al. confirmed that a peptide-incorporated nanofiber mat exhibited antibacterial performance comparable to that of a commercial silver-containing dressing [7]. These results show that AMPs can serve as effective antibacterial active components in nanofibers, while also suggesting that it is important to ensure that the active component remains on the surface after processing and ensuring consistent functional performance [8–11]. More recently, PVA-based functional nanofibers have been widely developed by incorporating inorganic nanoparticles, bioactive compounds, and secondary polymeric components to enhance their thermal stability, biological activity, and surface functionality for diverse biomedical applications [12–16]. However, studies employing recombinant bio-derived adhesive antimicrobial proteins as multifunctional additives in electrospun PVA nanofibers remain very limited. A comparison of representative antibacterial electrospun nanofibrous systems reported in the literature, including their polymer matrices, antibacterial components, fabrication methods, antibacterial performance, and stability-related characteristics, is provided in Table S1. This comparison further highlights the limited reports on recombinant bio-derived adhesive antimicrobial proteins incorporated directly into PVA nanofibers.

Along with this, research on fibrous biomaterials using mussel adhesive proteins and mussel-inspired chemistry is also attracting increasing attention. In a recent review, Dai et al. reported that MAP- and polydopamine (PDA)-based nanofibers are emerging as important platforms in the field of wound healing [17]. In addition, Kim et al. fabricated nanofibers using Fe(III)–DOPA complexes based on recombinant mussel adhesive protein (rfp-1) and polycaprolactone (PCL) [18]. That study showed that the stoichiometry of the Fe(III)–DOPA complex could be controlled through pH adjustment of the buffer solution and reported that the stiffness of the nanofibers increased linearly with increasing complex concentration. This study represents a significant example, demonstrating that mechanical properties can be precisely controlled through coordination chemistry in mussel adhesive protein-based nanofibers.

Meanwhile, poly(vinyl alcohol) (PVA) has been widely used as a matrix for electrospinning because of its high hydrophilicity and ease of processing, but its weak structural stability in humid environments has been continuously pointed out as a drawback [19]. Accordingly, in nanofiber applications based on PVA, water stabilization is regarded as an important post-treatment step, and stabilization strategies through heat treatment have been widely used [5]. However, PVA nanofibers containing functional recombinant proteins still need to be carefully examined to determine whether the protein-derived surface components and antibacterial activity are maintained after heat treatment. Recent studies have further highlighted the versatility of PVA-based materials fabricated by solvent casting and electrospinning for biomedical, filtration, and packaging applications. These studies also emphasize that appropriate stabilization strategies are essential for improving their structural integrity and functional performance [20–23].

Therefore, in this study, AMAP was directly incorporated into PVA and electrospun into nanofibers, followed by thermal treatment to investigate their water stability and surface-property changes. Notably, the incorporation of the AMAP alone, without additional antibacterial agents or inorganic additives, imparted antibacterial activity while simultaneously alleviating the inherent structural instability of PVA nanofibers in aqueous environments. By systematically evaluating the spinning behavior, morphological stability, surface characteristics, and antibacterial performance as a function of the AMAP content, we aimed to determine whether AMAP could retain its functionality after thermal treatment and serve as both an antibacterial component and a structural modifier of the PVA matrix.

2. Experimental

2.1. Synthesis of recombinant antimicrobial mussel adhesive protein (AMAP)

The recombinant antimicrobial mussel adhesive protein (AMAP) used in this study was designed by fusing a synthetic AMP to the C-terminus of MAP fp-151. The base scaffold, fp-151, is a recombinant fusion protein consisting of fp-1-type sequences attached to both the N- and C-termini of fp-5. The AMAP was synthesized using genetic recombination technology, where the corresponding gene was expressed in *Escherichia coli* (*E. coli*) and cultured in LB broth. The purified AMAP was purchased from Biovit (Seoul, South Korea). Protein expression was then induced with IPTG, and the cells were harvested. Using a cell disruptor and a centrifuge, the *E. coli* cell wall and the synthesized protein were separated. The lysed cell solution was then loaded onto a column packed with cation beads as the filler, and 25% acetic acid was passed through the column to isolate and purify only the mussel adhesive protein. To convert the L-tyrosine attached to the extracted protein into L-DOPA, the enzyme tyrosinase was used as a catalyst, thereby facilitating the conversion of L-tyrosine residues into L-DOPA and finally obtaining the fp-151 mussel adhesive protein.

2.2. Preparation of antimicrobial nanofiber

The PVA (>99% hydrolyzed, M_w = 89,000–98,000, Sigma Aldrich Co., USA) was used as the carrier polymer for spinning the antimicrobial adhesive protein. To prepare the spinning solution for the antibacterial nanofibers, PVA was added to the deionized water (D.I) and stirred at 60 ℃ for 3 h. At this time, the concentration of the spinning solution was set to 20 wt.%. The antimicrobial adhesive protein (AMAP) was separately dissolved in distilled water at 1, 3, and 5 wt% based on the weight of PVA and stirred for 2 h at room temperature. The resulting AMAP

solutions were then mixed with the pre-prepared PVA spinning solution through ex-situ blending under continuous stirring at room temperature to obtain a homogeneous PVA-AMAP spinning solution. Electrospinning was carried out to fabricate nanofibers from the prepared spinning solution composition. Electrospinning was conducted at room temperature and 40% relative humidity under the following conditions: needle gauge 18, solution feed rate of 1 mL h-1, voltage of 22.5 kV, and tip-collector distance (TCD) of 13 cm. Finally, the electrospun nanofibers were rendered insoluble by thermal treatment (120 °C for 2 h). The prepared samples were denoted as neat PVA, PVA-AMAP1, and PVA-AMAP5. The samples were designated according to the AMAP content and post-treatment condition. For example, PVA-AMAP1 represents a nanofiber web electrospun from a PVA solution containing 1 wt% AMAP, whereas PVA-AMAP1-T denotes the corresponding nanofiber web after thermal treatment.

2.3. Characterization

The molecular mass of the purified recombinant AMAP was determined by MALDI-TOF mass spectrometry in linear positive-ion mode using sinapinic acid and α-cyano-4-hydroxycinnamic acid as matrices. The purity of the purified AMAP was evaluated by SEC-HPLC using a TSKgel G3000SWXL column (7.8 × 300 mm) with 1 × PBS (pH 7.0) as the mobile phase at a flow rate of 0.5 mL min^{-1} and detection at 280 nm.

The PVA nanofiber samples were characterized by X-ray photoelectron spectroscopy (XPS, K-Alpha, ThermoFisher Scientific, USA) using a Mg Kα X-ray source with a 10 mA emission current and a 10 kV accelerating voltage. Fourier transform infrared (FT-IR, Nicolet iS10, Thermo Scientific) spectroscopic and wide-angle X-ray diffraction (WAXD, Thermo Scientific) measurements were performed to identify the structure of the neat PVA, PVA-AMAP1, and PVA-AMAP5 nanofibers before and after thermal treatment. The fiber morphology was then examined using field-emission scanning electron microscopy (FE-SEM, NOVA nanoSEM 450, FEI, USA) and energy dispersive X-ray (EDX) spectroscopy and the results were discussed in detail using Pt-coated samples. The fiber diameter and distribution were calculated from the SEM images using Image J software (National Institute of Health, USA). In addition, the thermal properties of the neat PVA, PVA-AMAP1, and PVA-AMAP5 nanofibers before and after thermal treatment were investigated by thermogravimetric analysis (TGA) and differential scanning calorimetry (DSC).

Thermal properties were analyzed by DSC using a Waters TA Instruments Discovery DSC 25 (30 to 275 °C, 10 °C/min). Samples were pre-dried at 30 °C for 3 h and tested under nitrogen (60 mL/min). Thermal stability was evaluated by TGA using a Waters TA Instruments Discovery TGA 55 (RT– 820 °C, 10 °C/min, N_2 at 90 mL/min).

The water resistance of the films was quantitatively evaluated by measuring the mass loss and mass retention after water immersion. For each sample, three film specimens with dimensions of 2 cm × 2 cm were prepared and individually weighed to determine their initial dry mass (M_0). The specimens were then immersed in distilled water for 1 h at room temperature. After immersion, the specimens were removed from the water and dried in a vacuum oven at 40–50 °C until a constant mass was obtained (M_1). The mass loss and mass retention were calculated using the following equations:

$$\text{Mass Loss}\,(\%) = \frac{M_0 - M_1}{M_0} X100$$

$$\textit{MassRetention}(\%) = 100 - \textit{Massloss}(\%)$$

The surface wettability of the nanofibers was evaluated by water contact angle measurements, and the water stability was assessed after immersion in water for 1 h. Mechanical properties were measured using a Instron 5567 Universal Testing Machine (100 N load cell, 25 mm gauge length, 5 mm/min). Film thickness was averaged from five measurements.

Finally, the antimicrobial activities of the neat PVA-T and PVA-AMAP5-T nanofibers were determined using *S. aureus* and *E-Coli*. Antimicrobial activity was evaluated according to the KS K 0693 and JIS L 1902 methods. Specimens were cut into 2 × 2 cm^2 pieces and placed in a 6-well plate as control and sample groups. Then, 0.2 mL of *S. aureus* and *E-Coli* suspension (1.3 × 10^3 CFU mL^{-1}) was inoculated onto each specimen. The inoculated control and sample specimens were incubated at 37 °C for 18 h. After incubation, 3 mL of PBS neutralizing solution was added to each well, and the wells were shaken sufficiently to uniformly disperse the bacteria. Then, 100 μL of the suspension was collected, spread onto TSB (Tryptic Soy Broth) medium, and incubated for 24 h to evaluate bacterial growth.

3. Results and discussion

A distinct protein band at approximately ~ 25 kDa was observed in the induced sample (Lane 2), indicating that recombinant antimicrobial mussel adhesive protein (AMAP) was successfully and stably expressed at the target molecular weight under the induction conditions (Fig. 1(a)). Fig. 1(b) shows a schematic representation of the chemical structure showing the primary sequence and major structural features of the AMAP. The model illustrates the fusion of a mussel adhesive protein-derived scaffold (gray surface) with a functional alpha-helical AMP domain (blue). The AMAP construct is characterized by a high density of tyrosine residues capable of forming catechol functional groups and cationic residues such as lysine, which synergistically provide both strong moisture-resistant adhesion and potent antimicrobial activity (Fig. 1(c)). This amphiphilic structure, which combines a mussel adhesive α-helix with an antimicrobial peptide domain, provides a structural basis for simultaneous adhesion and antibacterial activity.

The molecular mass of the recombinant AMAP was confirmed by MALDI-TOF MS (Fig. S1a). A single dominant signal was observed at *m/z* 25,654, which is in good agreement with the theoretical average mass of 25,470.3 Da calculated from the 219-residue sequence of the fp-151–antimicrobial peptide fusion. The deviation of approximately 184 Da corresponds to a relative mass error of 0.72%, supporting expected molecular mass of the recombinant AMAP. No major signals corresponding to the lower-molecular-mass species were observed, indicating that appreciable proteolytic degradation or truncation was not evident in the analyzed preparation. The purity of the recombinant AMAP was evaluated by SEC-HPLC (Fig. S1b). A single major peak was observed at approximately 25 min, with a calculated purity of 96.73% based on the peak area. Together, the MALDI-TOF MS and SEC-HPLC results confirm the expected molecular mass and high purity of the AMAP used for the fabrication of the antimicrobial nanofibers.

The surface morphology of nanofibers prepared by electrospinning solutions in which AMAP was introduced into PVA was observed by FE-SEM, as shown in Fig. 2(a–c). All samples exhibited a uniform and continuous fibrous structure, with no distinct beads observed within the observation range. In addition, the surfaces were found to be relatively smooth. The viscosities of the spinning solutions were measured using a Brookfield viscometer at 25 °C under a fixed spindle speed of 30 rpm. Based on the linear relationship between shear stress and shear rate, all solutions exhibited approximately Newtonian behavior within the measured range. The corresponding viscosities were 729.5 mPa·s for neat PVA, 904.6 mPa·s for PVA-AMAP1, and 702.2 mPa·s for PVA-AMAP5 (as shown in Fig. S2). The corresponding average fiber diameters of the electrospun nanofibers were 334 ± 49 nm for the neat PVA nanofiber web and 320 ± 29 and 350 ± 35 nm for the PVA-AMAP nanofiber webs (1 wt.% and 5 wt.%), respectively, indicating an average diameter distribution at about the 330 nm level as shown in Fig. 2d–f. Although the rheological behavior changed according to the viscosity variation of the electrospinning solutions, the difference in the diameters of the electrospun nanofibers was not large. The lack of significant correlation between solution viscosity and fiber diameter suggests that intermolecular interactions, such as hydrogen bonding

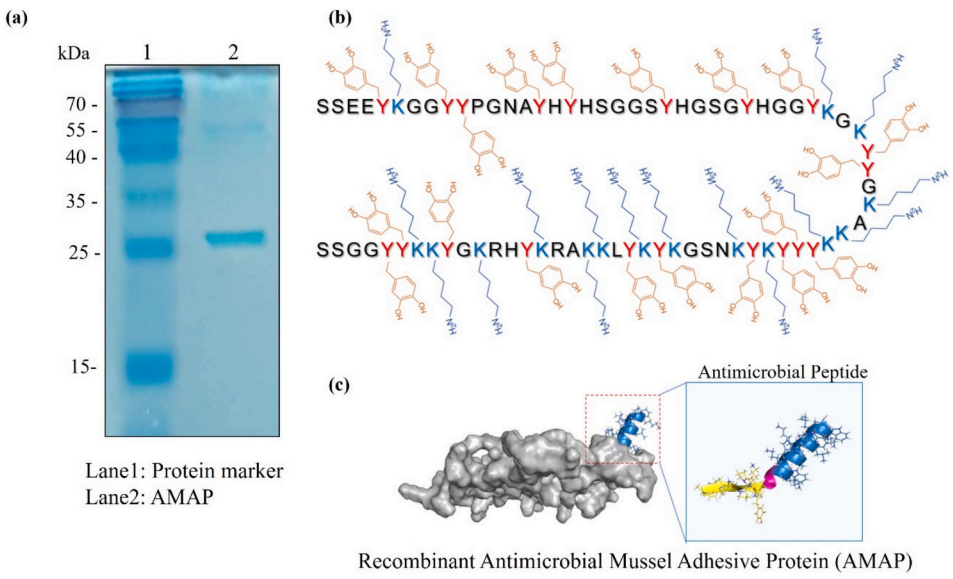


Fig. 1. (a) SDS-PAGE analysis. (b) Chemical structure. (c) Structural representation of the AMAP, respectively.

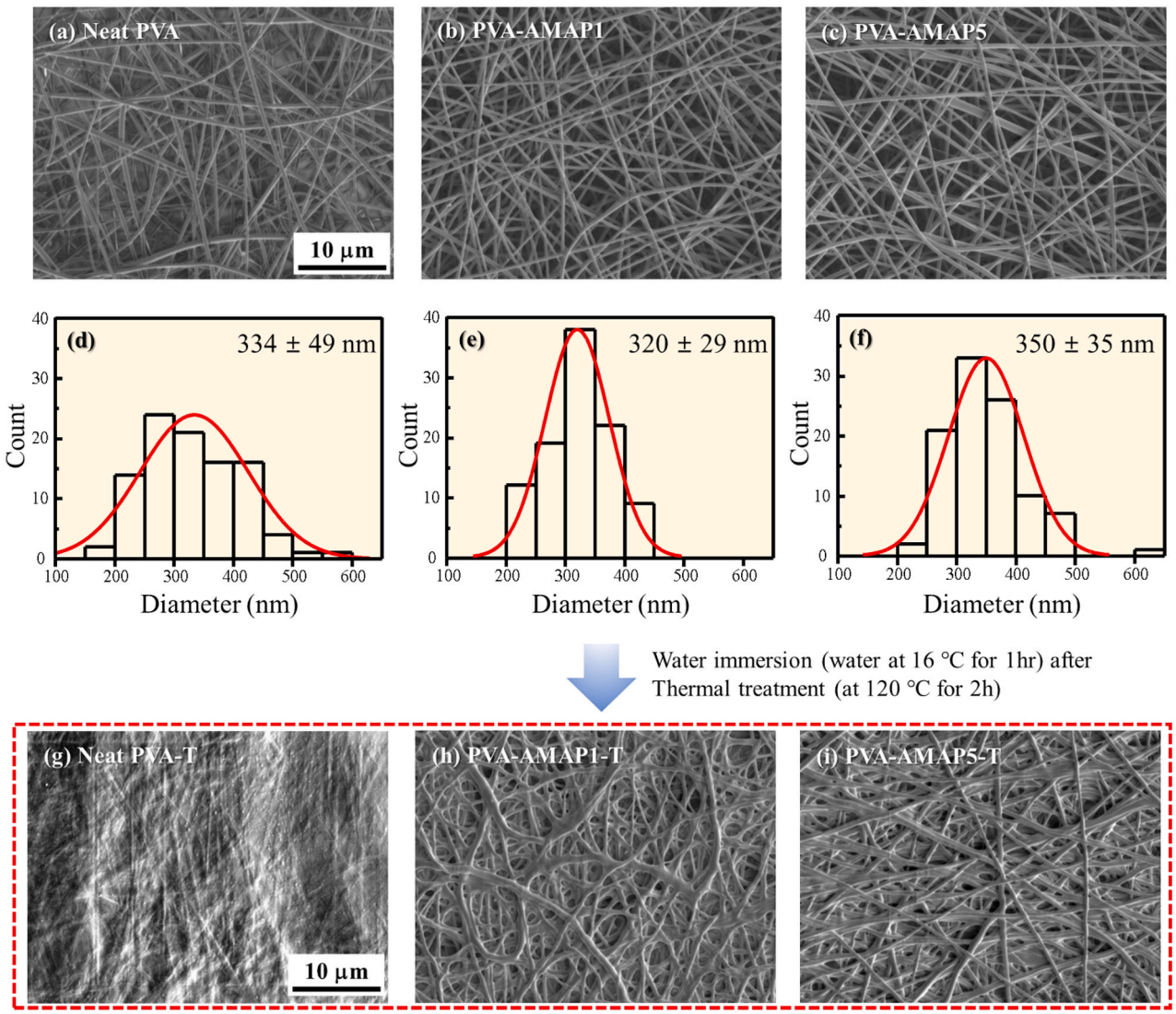


Fig. 2. Morphological characterization of AMAP-incorporated PVA nanofibers. (a-c) FE-SEM images, (d-f) nanofiber diameter distributions, (g-i) FE-SEM images of water immersion after thermal treatment, neat PVA, PVA-AMAP1, and PVA-AMAP5, respectively.

between AMAP and PVA, regulate the final fiber morphology during electrospinning.

To alleviate the structural vulnerability of PVA to deformation in moist environments, the electrospun nanofiber web was heat-treated in a vacuum oven at 120 ℃ for 2 h, and the structural deformation of the nanofibers was then examined through water immersion. FE-SEM images of the nanofiber web after thermal treatment and water immersion are shown in Fig. 2g–i. In the case of the AMAP-incorporated samples, it can be confirmed that a relatively stable nanoporous structure and fibrous morphology were maintained compared with the morphology before treatment. In contrast, the PVA sample without AMAP addition (Fig. 2g) showed a film-like shape in which the fiber structure collapsed, and the surface undulations were non-uniform. This behavior can be attributed to the relatively facile rehydration and swelling of neat PVA chains in the aqueous environment even after thermal treatment, resulting in fiber fusion and structural collapse. In contrast, AMAP-incorporated samples demonstrated improved structural stability due to synergistic effects of intermolecular interactions between AMAP and PVA and thermal treatment [24–26]. To further support these morphological observations, the water resistance of the films was quantitatively evaluated by determining the mass loss and mass retention after 1 h of water immersion followed by drying as shown in Fig. S3. The mass loss of PVA decreased from 69.35 ± 5.71% to 65.08 ± 3.02% after thermal treatment (PVA-T), corresponding to an increase in mass retention from 30.65 ± 5.71% to 34.92 ± 3.02%. Similarly, the mass loss of PVA-AMAP5 decreased from 77.86 ± 4.51% to 59.12 ± 6.14% after thermal treatment (PVA-AMAP5-T), while the mass retention increased from 22.14 ± 4.51% to 40.88 ± 6.14%. These results correspond to a reduction in mass loss of 4.27% for PVA and 18.74% for PVA-AMAP5, quantitatively confirming the improved resistance of the films to water-induced dissolution after thermal treatment.

The mechanical properties of the electrospun nanofiber pads were evaluated by tensile testing, and the corresponding stress–strain curves are shown in Fig. S4. Thermal treatment generally improved the tensile strength of the nanofiber pads. Among the AMAP-containing samples, PVA-AMAP3-T exhibited the highest tensile strength, which may be attributed to an optimum AMAP concentration that promotes effective intermolecular interactions and stress transfer within the PVA nanofibrous network. Interestingly, PVA-AMAP5-T also showed slightly higher tensile strength than PVA-T, which can be associated with additional interactions between AMAP and PVA that contribute to reinforcement of the nanofiber network. These results demonstrate that AMAP incorporation, particularly at an optimized concentration, can enhance the mechanical performance of thermally treated PVA nanofiber pads. The elongation at break was also analysed to further assess their mechanical flexibility and deformation behaviour.

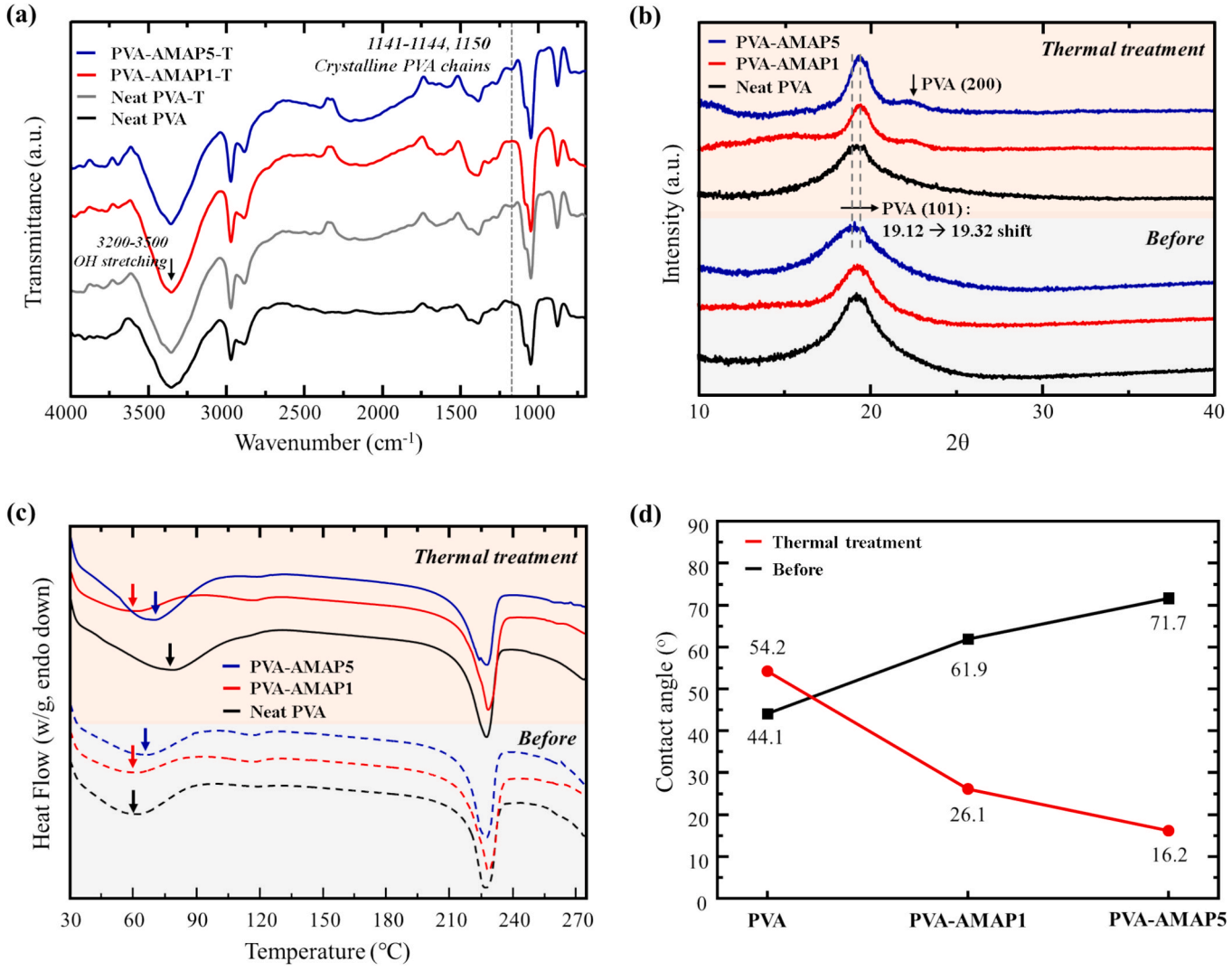


Fig. 3. Chemical and structural characterization of AMAP-incorporated nanofibers. (a) FT-IR spectra. (b) XRD patterns. (c) DSC thermograms. (d) Water contact angle. (e) EDS elemental mapping images and spectra. (f) XPS survey spectra of neat PVA, PVA-AMAP5, and PVA-AMAP5-T nanofibers before and after thermal treatment, respectively.

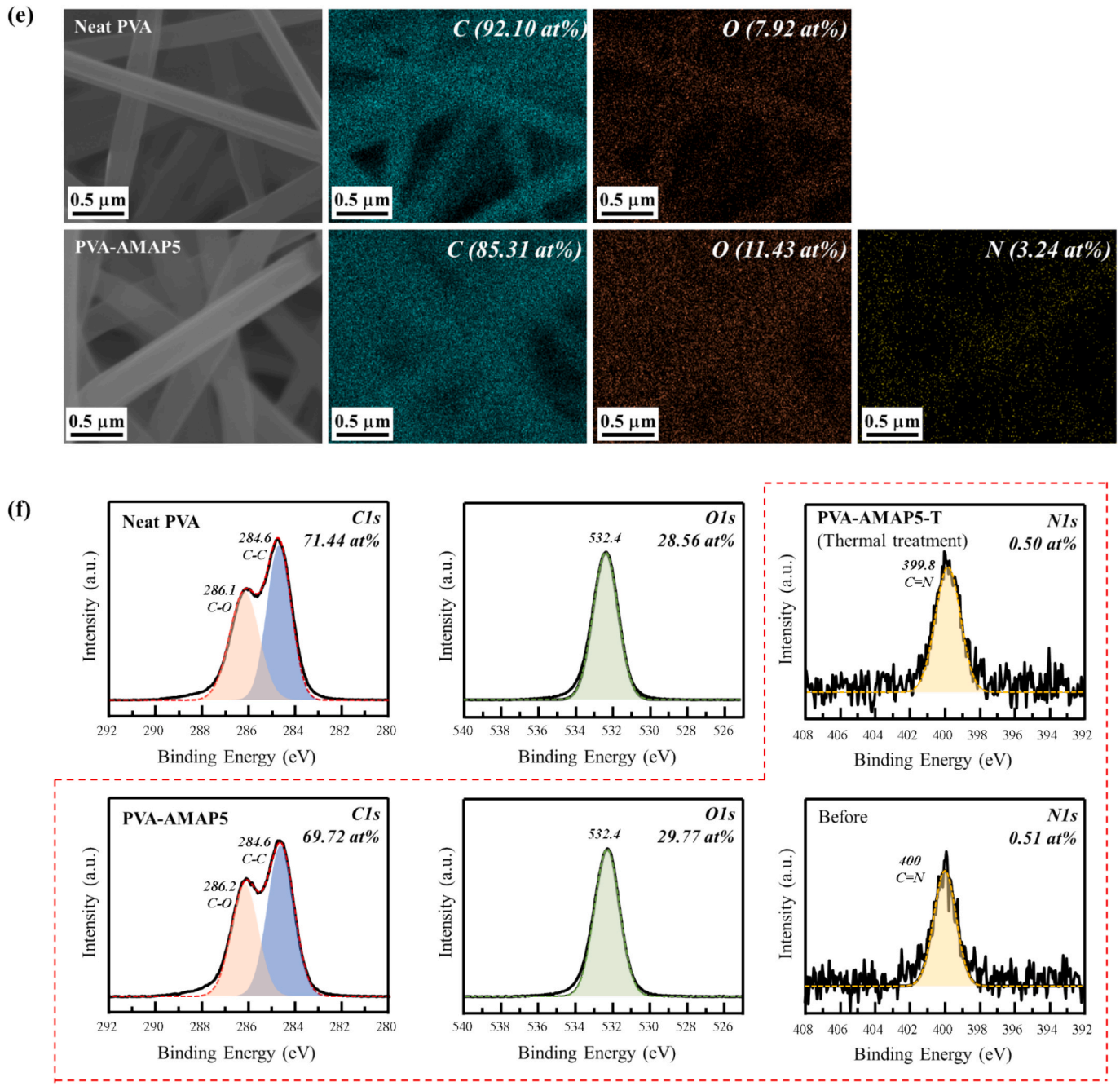


Fig. 3. (*continued*).

The structural changes of the nanofiber web before and after thermal treatment were analyzed by FT-IR and XRD, as shown in Fig. 3a and b. In the FT-IR spectra, a change in the relative intensity of the peak near 1141–1144 cm^{-1}, associated with the crystalline C-O vibration of PVA, was observed after thermal treatment. In addition, in XRD, it can be seen that the diffraction peak near $2\theta = 19.12°$ corresponding to the (101) plane of PVA increased in intensity after thermal treatment and shifted to 19.32°. Furthermore, in the AMAP-added samples, the diffraction corresponding to the (200) plane of PVA appeared more clearly after thermal treatment, while the basic semicrystalline structure of PVA was maintained. From the XRD results, the calculated FWHM values of the diffraction peak for the (101) plane of neat PVA before and after thermal treatment were 2.14° and 2.09°, respectively, showing no significant difference. In contrast, those of PVA-AMAP1 and PVA-AMAP5 decreased from 2.12° to 1.37° and from 2.61° to 1.40°, respectively. In addition, the relative area ratio of the diffraction component for the (200) plane increased from 9.6% to 21.8% for PVA-AMAP1 and from 12.4% to 24.5% for PVA-AMAP5. These results indicate that, during the thermal treatment process, the removal of residual moisture together with the promotion of hydrogen bonding between PVA chains and rearrangement of the molecular chains, resulted in the formation of a more ordered structure. In addition, it can be considered that the introduction of AMAP further promoted intermolecular interactions with PVA and thereby affected structural rearrangement.

The thermal properties of the fabricated nanofiber webs were evaluated by DSC and TGA, as shown in Figs. 3(c) and S5. First, examining the DSC results (Fig. 3(c)), the Tg of neat PVA was confirmed to be 76.4 ℃, whereas in the nanofiber webs containing 1 wt.% and 5 wt.% AMAP, it was somewhat decreased to 62.1 ℃ and 68.7 ℃, respectively. Notably, as the AMAP content increased, the Tg exhibited an increasing

trend. This behavior is considered to be attributed to the strong hydrogen bonding effect between the functionalized NH groups in AMAP and the PVA matrix, which effectively restricts the mobility of the polymer chains. In contrast, the Tm (melting point) did not change significantly with AMAP addition. However, when Tg was evaluated after thermal treatment, neat PVA showed a significant decrease to 61.6 ℃, corresponding to a decrease of about 14.8 ℃, whereas in the AMAP-added samples, the decrease was slight, within about 2–7% compared with before thermal treatment. From the TGA results (Fig. S5), it can be seen that the initial thermal decomposition onset temperature increased to a higher temperature with AMAP addition, and in particular, the maximum decomposition characteristic temperature of PVA-AMAP5 shifted from 276.2 ℃ to 283.6 ℃ after thermal treatment. This indicates that the thermal stability of the PVA-AMAP5 sample was partially improved by thermal treatment, which is also attributed to the strong hydrogen bonding interactions between AMAP and the PVA matrix that enhance the overall thermal resistance of the structure. The surface wettability of the PVA nanofiber webs before and after thermal treatment and according to AMAP incorporation was evaluated by contact-angle measurements, as shown in Fig. 3(d). As AMAP was introduced, the contact angle of neat PVA gradually increased from 44.1° to 61.9° for PVA-AMAP1 and to 71.7° for PVA-AMAP5, showing a decrease in surface energy and an increase in hydrophobicity. However, the behavior after thermal treatment showed the opposite tendency, with neat PVA increased to 54.2°, whereas PVA-AMAP1 and PVA-AMAP5 decreased markedly to 26.1° and 16.2°, respectively. This behavior can be explained by the molecular structure of the AMAP used in this study. As confirmed from the molecular structure of AMAP in Fig. 1(b), it has a typical amphiphilic structure that simultaneously includes hydrophilic residues (the catechol group of DOPA, the amine group of lysine, and the hydroxyl groups of serine/threonine) and hydrophobic moieties (the indole group of tryptophan, the pyrrolidine group of proline, and aliphatic alanine/glycine residues). Therefore, immediately after electrospinning, as the hydrophobic part preferentially moves to the nanofiber surface due to minimization of surface energy, it can be interpreted that the surface became more hydrophobic as the AMAP content increased [27,28]. After thermal treatment, a clear reversal in wettability was observed, which can be attributed to the thermally induced surface rearrangement of AMAP. During this process, hydrophobic segments are incorporated into the PVA crystalline domains, while hydrophilic functional groups (e.g., catechol and amine groups) preferentially orient toward the fiber surface [29–31]. Furthermore, physical crosslinking between the catechol groups of AMAP and the –OH groups of PVA contributes to the enhanced hydrophilicity and structural stability [32–34]. To obtain experimental evidence for the proposed thermally induced surface rearrangement, angle-resolved X-ray photoelectron spectroscopy (AR-XPS) was performed on the four samples i.e neat PVA, PVA-T, PVA-AMAP5, and PVA-AMAP5-T over different angular conditions of 0–85°, where 0° represents the relatively deeper-sensitive condition and 85° represents the most surface-sensitive condition. The C and O atomic concentrations for neat PVA ranged from 68.02 to 69.30 at.% and 30.70–31.98 at.%, respectively, corresponding to an angular variation of ~ 0.24 at.% for both C and O between 0° and 85°. Similarly, PVA-T showed C and O concentrations ranging from 68.56 to 70.25 at.% and 29.75–31.44 at.%, respectively, corresponding to an angular variation of ~ 0.90 at.% for both C and O. In contrast, PVA-AMAP5 showed C and O concentrations of 67.51–71.60 at.% and 26.99–31.74 at.%, respectively, corresponding to angular variations of ~ 4.1–4.4 at.% for C and O. Likewise, PVA-AMAP5-T exhibited C and O concentrations of 66.83–70.87 at.% and 27.82–32.61 at.%, respectively, corresponding to angular variations of ~ 4.0–4.8 at.% for C and O. Since nitrogen is associated with the AMAP component and is not a major constituent of the PVA backbone, the N signal was considered as an AMAP-sensitive marker. The N concentration ranged from 0.75 to 1.09 at.% for PVA-AMAP5 and 0.56–1.31 at.% for PVA-AMAP5-T. Furthermore, the N/C atomic ratio increased from 0.011 to 0.015 for PVA-AMAP5, corresponding to ~ 37% increase, while PVA-AMAP5-T showed an increase from 0.008 to 0.018, corresponding to ~ 121% increase, between 0° and 85°. These results demonstrate that the AMAP-containing samples exhibit substantially greater depth-dependent changes in surface composition than the neat PVA controls, with the effect being particularly pronounced after thermal treatment. Although some angular fluctuations were observed in the N signal, the overall AR-XPS results support a thermally induced redistribution/reorganization of the AMAP-containing component within the near-surface region. This redistribution is consistent with the experimentally observed wettability reversal from hydrophobic to hydrophilic behavior. The complete AR-XPS spectra and quantitative angular data are provided in the Supporting Information (Figs. S6–S8).

The FE-SEM EDX and XPS analyses in Fig. 3(e and f) were performed to qualitatively evaluate the surface functionalization of the PVA nanofiber web according to AMAP incorporation. In the EDX analysis, only C and O components were observed in neat PVA, whereas an N component of 3.24 at% was detected in PVA-AMAP5 (Fig. 3(e)). This supports that protein- or peptide-derived components containing nitrogen were introduced into the nanofibers. A similar trend was also observed in the XPS analysis. No N1s signal was detected in neat PVA, whereas in PVA-AMAP5 and PVA-AMAP5-T (thermal treatment), the atomic ratio of N1s was observed at about 0.51–0.65 at.% and 0.50–0.54 at.%, respectively. These results suggest that the protein-derived surface components were not completely removed even after thermal treatment and remained on the surface. From the XPS results (Figs. 3(f) and S9), C1s and O1s peaks near 284.6 eV and 532.4 eV were identified in both neat PVA and PVA-AMAP5, and the C–C peak near 284.6 eV and the C-O-related peak near 286.1–286.2 eV were commonly observed in all samples. In contrast, in PVA-AMAP5, a binding energy peak of N1s was identified near 400 eV, and deconvolution analysis indicated that this was an AMAP-derived nitrogen component including a C=N component. The persistent N1s peak and stable nitrogen content (~0.50 at.%) after thermal treatment confirm that AMAP was stably maintained on the nanofiber surface.

The antibacterial efficacy against *S. aureus* and *E. coli* was evaluated using KSK 0693 standard, as shown in the Figs. 4 and S10. The blank and neat PVA (control) samples showed no reduction in bacterial survival and thus no distinct antibacterial effect against either bacterial strain.

In contrast, PVA-AMAP5-T showed excellent antibacterial activity, with a bacterial reduction rate of 96.0% against *S. aureus* and 92.9% against *E. coli*. Importantly, because these antibacterial measurements were performed after thermal treatment at 120 °C for 2 h, the observed activity provides direct functional evidence that the thermal treatment did not abolish the AMAP-derived antibacterial functionality. After storage under ambient conditions for 30 days, the bacterial reduction remained at 91.3% and 87.5% against *S. aureus* and *E. coli*, respectively, demonstrating that the antibacterial performance was largely preserved after the tested storage period. The slightly lower antibacterial reduction observed for *E. coli* compared with *S. aureus* may be associated with the more complex cell-envelope structure of Gram-negative bacteria, particularly the presence of an additional outer membrane that can act as a permeability barrier. It should be noted that the 30-day antibacterial stability evaluated in this study represents storage stability under ambient dry conditions. Although the antibacterial activity was retained after 30 days, quantitative AMAP release or leaching from the nanofibers was not investigated in the present study. The XPS results confirmed the presence of the AMAP-associated nitrogen signal after thermal treatment; however, this does not directly quantify AMAP release into an aqueous medium. Therefore, the retained antibacterial activity after 30 days is considered as storage stability during the tested period rather than direct evidence of AMAP non-leaching or long-term retention within the nanofibers. Future studies will investigate the long-term stability and antibacterial performance of the developed PVA-AMAP nanofibers under physiologically relevant conditions (e.g., PBS at 37 °C) along with quantitative AMAP release/leaching analysis and

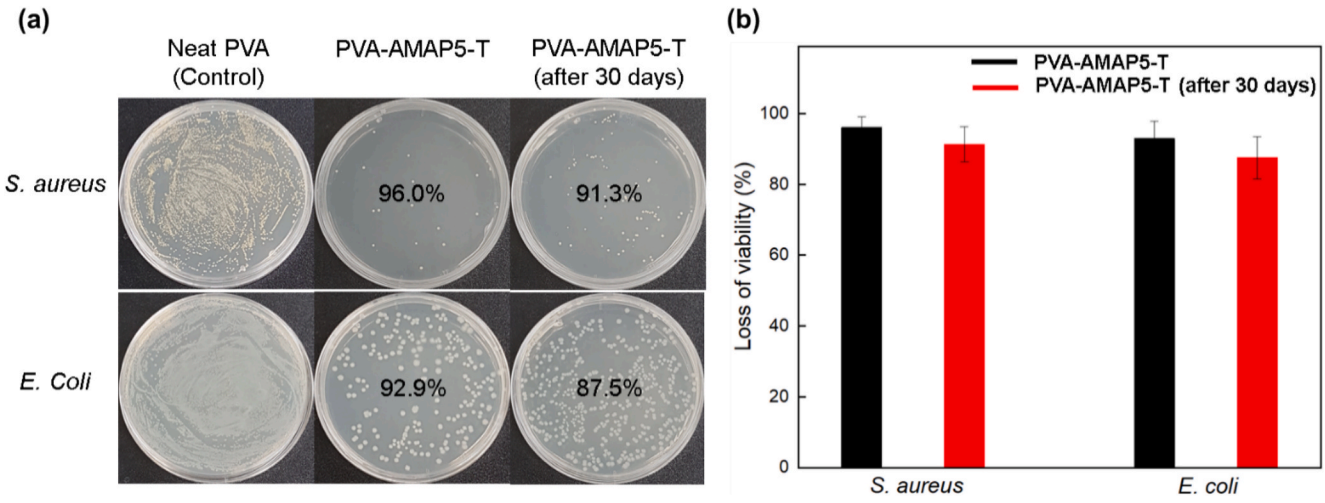


Fig. 4. Antibacterial activity against *S. aureus* and *E. coli* for neat PVA and heat-treated PVA-AMAP5-T nanofibers before and after storage at room temperature for 30 days, evaluated according to KSK 0693. (a) Representative colony images; (b) loss of bacterial viability (%). Values are mean ± SD (n = 3).

accelerated aging protocols to further assess their suitability for biomedical applications.

The antibacterial activity of PVA-AMAP5-T is tentatively attributed primarily to the cationic amphipathic AMP domain of AMAP. The lysine-rich AMP sequence may initially associate electrostatically with the polyanionic teichoic acids and negatively charged membrane components of *S. aureus* [35,36]. Subsequent interaction of the amphipathic peptide domain with the cytoplasmic membrane may disturb lipid packing, increase membrane permeability, induce membrane depolarization and ion leakage, and ultimately cause bacterial death [36,37]. The DOPA-derived catechol groups are not considered the principal killing moiety; instead, they may promote AMAP retention and interfacial association within the PVA nanofibers, thereby maintaining the surface accessibility of the AMP domain. Similar catechol-functionalized antimicrobial systems have shown that catechol primarily supports surface immobilization, whereas cationic amphiphilic groups mediate membrane-active contact killing [38]. Because membrane damage and AMAP release were not directly measured in this study, this pathway is proposed based on the AMAP structure and relevant literature.

Although the present results demonstrate antibacterial performance and structural stability of PVA-AMAP nanofibers, the objective of this study was to establish the feasibility of incorporating AMAP into electrospun PVA nanofibers while retaining its antibacterial functionality after thermal treatment. Consequently, comprehensive biological evaluations, including cytocompatibility, cell viability and hemocompatibility, remain necessary to fully validate the suitability of this material for biomedical applications, such as wound dressings.

Fig. 5 schematically illustrates the structural rearrangement of PVA-AMAP nanofibers induced by thermal treatment. In the as-spun state, AMAP is distributed randomly within the amorphous PVA matrix. During thermal treatment, the ordering of PVA chains into crystalline regions drives the repositioning of AMAP due to its amphiphilic nature. This rearranged structure stably retains AMAP within the nanofibers, suppressing its loss and contributing to the sustained antibacterial

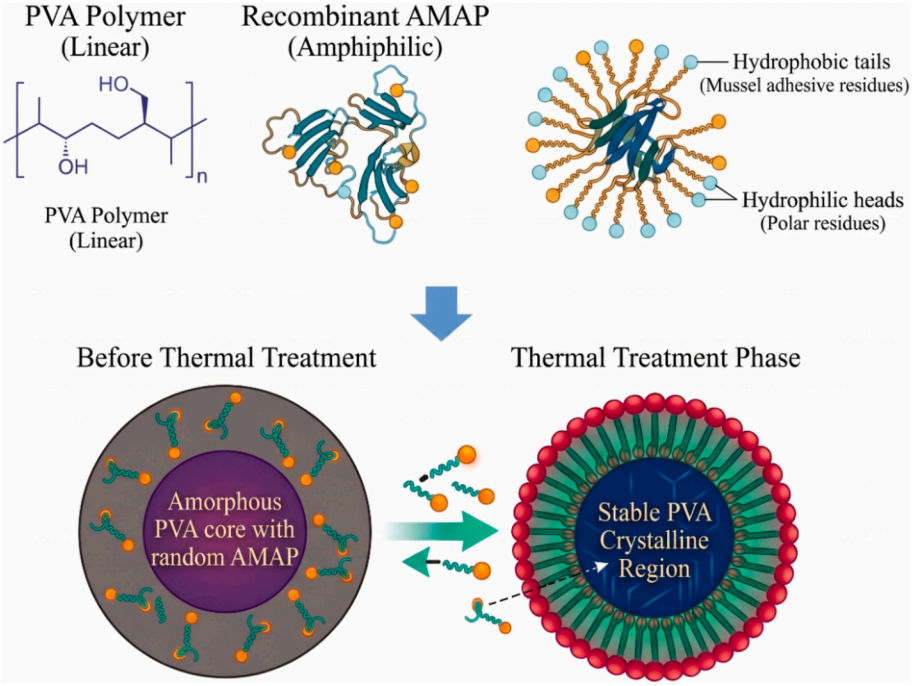


Fig. 5. Proposed mechanism for the structural rearrangement of PVA-AMAP nanofibers during thermal treatment.

activity observed over 30 days.

4. Conclusion

In this study, a recombinant antimicrobial mussel adhesive protein (AMAP) with an amphiphilic structure was synthesized and incorporated into a PVA matrix to fabricate electrospun nanofibers. The incorporation of AMAP did not significantly affect the average fiber diameter, while notably enhancing the structural stability of the nanofibers under water immersion conditions after thermal treatment compared to neat PVA. This stabilizing effect became more pronounced with increasing AMAP content. Structural analyses revealed thermally induced rearrangement of PVA chains and increased molecular ordering. The XPS and AR-XPS analysis confirmed the presence of AMAP-derived nitrogen species, including a C=N component, even after thermal treatment, indicating the retention of AMAP near the nanofiber surface. Contact-angle measurements showed a significant transition in surface wettability for the PVA-AMAP5 sample, from hydrophobic (71.7°) to hydrophilic (16.2°) after thermal treatment. This drastic change is attributed to surface rearrangement driven by the amphiphilic nature of AMAP, where hydrophobic domains are stabilized within the fiber matrix through interactions with the PVA crystalline regions, while hydrophilic functional groups are preferentially oriented toward the fiber surface. The mechanical strength results further demonstrated that the incorporation of AMAP maintained the mechanical performance of the PVA nanofiber mats, with AMAP-containing samples showing tensile properties comparable to the thermally treated PVA matrix. Finally, the thermally treated PVA-AMAP5 nanofibers exhibited a bacterial reduction rate of 96.0% against *S. aureus* and 92.9% against *E. coli*, while maintaining 91.3% and 87.5% antibacterial activity against *S. aureus* and *E. coli*, respectively, after 30 days of storage under ambient conditions. These results demonstrate that the AMAP incorporation enables the simultaneous enhancement of structural stability and surface functionality, providing a promising strategy for durable antibacterial nanofiber platforms.

CRediT authorship contribution statement

Daun Lim: Writing – original draft, Formal analysis, Conceptualization. **Young Nam Kim:** Writing – original draft, Investigation. **Kundan Singh Rawat:** Writing – review & editing. **Won-Hui Jeong:** Methodology, Investigation. **Somi Yoon:** Investigation. **Jeong Jae Wie:** Writing – review & editing, Investigation. **Eun-Bin Chu:** Investigation, Formal analysis. **Yong-Tae Kim:** Validation, Methodology. **Yoong Ahm Kim:** Validation, Supervision. **Yong Chae Jung:** Writing – review & editing, Supervision, Project administration, Funding acquisition.

Declaration of competing interest

The authors declare that they have no known competing financial interests or personal relationships that could have appeared to influence the work reported in this paper.

Acknowledgements

This work was supported by the National R&D Program through the National Research Council of Science & Technology (NST) grant by the Korea government (MSIT) (CRC23014-000). J.J.W acknowledges the financial support from the Bio&Medical Technology Development Program of the National Research Foundation (NRF) funded by the Korean government (MSIT) (No. RS-2024-00451875). Y.A.K acknowledges the financial support from the ITECH R&D Program of the Ministry of Trade, Industry and Energy (MOTIE), Korea, through the Korea Evaluation Institute of Industrial Technology (KEIT) (RS-2023-00257573).

Appendix A. Supplementary data

Supplementary data to this article can be found online at https://doi.org/10.1016/j.eurpolymj.2026.115076.

Data availability

The data supporting the findings of this study are available from the corresponding author upon reasonable request.

References

[1] H.P. Felgueiras, M.T.P. Amorim, Functionalization of electrospun polymeric wound dressings with antimicrobial peptides, Colloids Surf. B Biointerfaces 156 (2017) 133–148, https://doi.org/10.1016/j.colsurfb.2017.05.001.
[2] S.P. Miguel, D.R. Figueira, D. Simões, M.P. Ribeiro, P. Coutinho, P. Ferreira, I. J. Correia, Electrospun polymeric nanofibres as wound dressings: a review, Colloids Surf. B Biointerfaces 169 (2018) 60–71, https://doi.org/10.1016/j.colsurfb.2018.05.011.
[3] S. Homaeigohar, A.R. Boccaccini, Antibacterial biohybrid nanofibers for wound dressings, Acta Biomater. 107 (2020) 25–49, https://doi.org/10.1016/j.actbio.2020.02.022.
[4] S. Parham, A.Z. Kharazi, H.R. Bakhsheshi-Rad, M. Kharaziha, A.F. Ismail, S. Sharif, M. Razzaghi, S. Ramakrishna, F. Berto, Antimicrobial synthetic and natural polymeric nanofibers as wound dressing: a review, Adv. Eng. Mater. 24 (2022) 2101460, https://doi.org/10.1002/adem.202101460.
[5] W.J.A. Homer, M. Lisnenko, A.C. Gardner, E.K. Kostakova, J. Valtera, I.B. Wall, V. Jencova, P.D. Topham, E. Theodosiou, Assessment of thermally stabilized electrospun poly (vinyl alcohol) materials as cell permeable membranes for a novel blood salvage device, Biomater. Adv. 144 (2023) 213197, https://doi.org/10.1016/j.bioadv.2022.213197.
[6] D.W. Song, S.H. Kim, H.H. Kim, K.H. Lee, C.S. Ki, Y.H. Park, Multi-biofunction of antimicrobial peptide-immobilized silk fibroin nanofiber membrane: Implications for wound healing, Acta Biomater. 39 (2016) 146–155, https://doi.org/10.1016/j.actbio.2016.05.008.
[7] Q. Yang, S. Cui, X. Song, J. Hu, Y. Zhou, Y. Liu, An antimicrobial peptide-immobilized nanofiber mat with superior performances than the commercial silver-containing dressing, Mater. Sci. Eng. C 119 (2021) 111608, https://doi.org/10.1016/j.msec.2020.111608.
[8] Y.K. Jo, J.H. Seo, B.H. Choi, B.J. Kim, H.H. Shin, B.H. Hwang, H.J. Cha, Surface-independent antibacterial coating using silver nanoparticle-generating engineered mussel glue, ACS Appl. Mater. Interfaces 6 (22) (2014) 20242–20253, https://doi.org/10.1021/am505784k.
[9] Z. Wang, X. Li, H. Chen, J. Du, L. Huang, T. Xin, M. Ma, W. Zhu, P. Zheng, C. Nie, Self-assembled nanostructured antimicrobial peptides: design strategies, structures, mechanism and therapeutic applications, J. Mater. Chem. B 13 (2025) 14593–14638, https://doi.org/10.1039/D5TB01872B.
[10] N. Saleem, N. Kumar, E. El-Omar, M. Willcox, X.T. Jiang, Nano-antimicrobial peptides (Nano-AMPs) to combat resistant gram-negative bacteria, Drug Deliv. Transl. Res. (2026) 1–35, https://doi.org/10.1007/s13346-026-02085-x.
[11] S. Kim, N.H. Kim, Z.H. Khaleel, D.H. Sa, D. Choi, S. Ga, C.G. Kim, J. Jang, K. Kim, Y.J. Kim, Mussel-inspired recombinant adhesive protein-based functionalization for consistent and effective antimicrobial treatment in chronic inflammatory skin diseases, Adv. Ther. 7 (4) (2024) 2300353, https://doi.org/10.1002/adtp.202300353.
[12] I. Erol, A. Dere, M. Yalcin, G. Khamidov, S.A. Mansour, D. Tukhtaev, S. Tillayev, F. Yakuphanoglu, Dielectric properties of novel nanocomposites based on PVA incorporating CuO nanoparticles, J. Mater. Sci.: Mater. Electron. 36 (16) (2025) 988, https://doi.org/10.1007/s10854-025-14942-5.
[13] G. Khamidov, O. Hazman, I. Erol, Thermal and biological properties of novel sodium carboxymethylcellulose-PPFMA nanocomposites containing biosynthesized Ag-ZnO hybrid filler, Int. J. Biol. Macromol. 257 (2024) 128447, https://doi.org/10.1016/j.ijbiomac.2023.128447.
[14] Erol, O. Hazman, F. Yılmaz, G. Khamidov, Enhanced biological, thermal and dielectric properties of polyvinyl alcohol by a methacrylate polymer and green synthesized silver nanoparticles, J. Polym. Environ. 33 (5) (2025) 2173–2192, https://doi.org/10.1007/s10924-025-03516-5.
[15] I. Erol, I. Ismail, M. Aksu, O. Hazman, Electrospun polyvinyl alcohol-chitosan/LaB6 fiber nanocomposites: synergistic enhancement of thermal, surface, dielectric, and bioactive properties, Int. J. Biol. Macromol. 331 (2025) 148386, https://doi.org/10.1016/j.ijbiomac.2025.148386.
[16] I. Erol, I. Ismail, O. Hazman, G. Khamidov, B. Güney, Multifunctional polyvinyl alcohol–sodium carboxymethyl cellulose/quercetin–ZnO nanofiber composites: synergistic interplay of bioactivity, conductivity, and surface engineering, Int. J. Biol. Macromol. 365 (2026) 152342, https://doi.org/10.1016/j.ijbiomac.2026.152342.
[17] Q. Dai, H. Liu, C. Gao, W. Sun, C. Lu, Y. Zhang, W. Cai, H. Qiao, A. Jin, Y. Wang, Y. Liu, Ad vances in mussel adhesion proteins and mussel-inspired material electrospun nanofibers for their application in wound repair, ACS Biomater Sci. Eng. 10 (10) (2024) 6097–6119, https://doi.org/10.1021/acsbiomaterials.4c01378.

[18] B.J. Kim, S. Kim, D.X. Oh, A. Masic, H.J. Cha, D. Hwang, Mussel-inspired adhesive protein-based electrospun nanofibers reinforced by Fe (III)–DOPA complexation, J. Mater. Chem. B 3 (1) (2015) 112–118, https://doi.org/10.1039/C4TB01496K.
[19] G.C. Türkoğlu, N. Khomarloo, E. Mohsenzadeh, D.N. Gospodinova, M. Neznakomova, F. Salaün, PVA-based electrospun materials-a promising route to designing nanofiber mats with desired morphological shape-a review, Int. J. Mol. Sci. 25 (3) (2024) 1668, https://doi.org/10.3390/ijms25031668.
[20] A. Turanli, C. Altinkok, E.C. Kacakgil, C. Dizman, G. Acik, A comprehensive study on the comparison between casted films and electrospun nanofibers of poly (vinyl alcohol)/chitosan blends: wettability, thermal, antioxidant, and adsorbent properties, Int. J. Biol. Macromol. 315 (2025) 144467, https://doi.org/10.1016/j.ijbiomac.2025.144467.
[21] G. Ciarleglio, N. Capuccilli, E. Toto, M.G. Santonicola, Poly (vinyl alcohol)/hyaluronic acid nanofibers for biomedical use under physiological conditions: Electrospinning fabrication and stabilization via solvent-free citric acid crosslinking, Polymers 18 (1) (2025) 79, https://doi.org/10.3390/polym18010079.
[22] M. Alonso-González, A. Corral-González, M. Felix, A. Romero, J.E. Martin-Alfonso, Developing active poly (vinyl alcohol)-based membranes with encapsulated antimicrobial enzymes via electrospinning for food packaging, Int. J. Biol. Macromol. 162 (2020) 913–921, https://doi.org/10.1016/j.ijbiomac.2020.06.217.
[23] C. Altinkok, G. Sagdic, O. Daglar, M.E. Ayra, Y.Y. Durmaz, H. Durmaz, G. Acik, A new strategy for direct solution electrospinning of phosphorylated poly (vinyl chloride)/polyethyleneimine blend in alcohol media, Eur. Polym. J. 183 (2023) 111750, https://doi.org/10.1016/j.eurpolymj.2022.111750.
[24] J.C. Park, T. Ito, K.O. Kim, K.W. Kim, B.S. Kim, M.S. Khil, H.Y. Kim, I.S. Kim, Electrospun poly (vinyl alcohol) nanofibers: effects of degree of hydrolysis and enhanced water stability, Polym. J. 42 (3) (2010) 273–276, https://doi.org/10.1038/pj.2009.340.
[25] M. Miraftab, A.N. Saifullah, A. Çay, Physical stabilisation of electrospun poly (vinyl alcohol) nanofibres: comparative study on methanol and heat-based crosslinking, J. Mater. Sci. 50 (4) (2015) 1943–1957, https://doi.org/10.1007/s10853-014-8759-1.
[26] Q. Zhang, Q. Li, L. Zhang, S. Wang, D.P. Harper, Q. Wu, T.M. Young, Preparation of electrospun nanofibrous poly (vinyl alcohol)/cellulose nanocrystals air filter for efficient particulate matter removal with repetitive usage capability via facile heat treatment, Chem. Eng. J. 399 (2020) 125768, https://doi.org/10.1016/j.cej.2020.125768.
[27] Y.J. Lai, P.C. Oh, T.L. Chew, A.L. Ahmad, Surface repellency beyond hydrophobicity: a review on the latest innovations in superomniphobic surfaces, ACS Omega 10 (6) (2025) 5172–5192, https://doi.org/10.1021/acsomega.4c08269.
[28] W. Zhao, Y. Wang, M. Han, J. Xu, K.C. Tam, Surface modification, topographic design and applications of superhydrophobic systems, Chem Eur J 28 (68) (2022) e202202657, https://doi.org/10.1002/chem.202202657.
[29] G. Bovone, O.Y. Dudaryeva, B. Marco-Dufort, M.W. Tibbitt, Engineering hydrogel adhesion for biomedical applications via chemical design of the junction, ACS Biomater Sci. Eng. 7 (9) (2021) 4048–4076, https://doi.org/10.1021/acsbiomaterials.0c01677.
[30] S. Tang, K. Feng, R. Yang, Y. Cheng, M. Chen, H. Zhang, N. Shi, Z. Wei, H. Ren, Y. Ma, Multifunctional adhesive hydrogels: from design to biomedical applications, Adv. Healthc. Mater. 14 (2) (2025) 2403734, https://doi.org/10.1002/adhm.202403734.
[31] H. Choi, K. Lee, Crosslinking mechanisms of phenol, catechol, and gallol for synthetic polyphenols: a comparative review, Appl. Sci. 12 (22) (2022) 11626, https://doi.org/10.3390/app122211626.
[32] Y. Chen, P. Ni, R. Xu, X. Wang, C. Fu, K. Wan, Y. Fang, H. Liu, Y. Weng, Tough and on-demand detachable wet tissue adhesive hydrogel made from catechol derivatives with a long aliphatic side chain, Adv. Healthc. Mater. 12 (29) (2023) 2301913, https://doi.org/10.1002/adhm.202301913.
[33] W. Zhang, R. Wang, Z. Sun, X. Zhu, Q. Zhao, T. Zhang, A. Cholewinski, F.K. Yang, B. Zhao, R. Pinnaratip, P.K. Forooshani, Catechol-functionalized hydrogels: biomimetic design, adhesion mechanism, and biomedical applications, Chem. Soc. Rev. 49 (2) (2020) 433–464, https://doi.org/10.1039/c9cs00285e.
[34] L. Prozorovska, B.A. Baker, P.E. Laibinis, G.K. Jennings, Surface-initiated, catechol-containing polymer films for effective chelation of aluminum ions, Langmuir 37 (46) (2021) 13617–13626, https://doi.org/10.1021/acs.langmuir.1c02112.
[35] T. Koprivnjak, C. Weidenmaier, A. Peschel, J.P. Weiss, Wall teichoic acid deficiency in *S. aureus* confers selective resistance to mammalian group IIA phospholipase A2 and human β-defensin 3, Infect. Immun. 76 (5) (2008) 2169–2176, https://doi.org/10.1128/IAI.01705-07.
[36] X. Yang, E. Huang, A.E. Yousef, Brevibacillin, a cationic lipopeptide that binds to lipoteichoic acid and subsequently disrupts cytoplasmic membrane of *S. aureus*, Microbiol. Res. 195 (2017) 18–23, https://doi.org/10.1016/j.micres.2016.11.002.
[37] P. Piller, H. Wolinski, R.A. Cordfunke, J.W. Drijfhout, S. Keller, K. Lohner, N. Malanovic, Membrane activity of LL-37 derived antimicrobial peptides against Enterococcus hirae: superiority of SAAP-148 over OP-145, Biomolecules 12 (4) (2022) 523, https://doi.org/10.3390/biom12040523.
[38] H. Han, J. Wu, C.W. Avery, M. Mizutani, X. Jiang, M. Kamigaito, Z. Chen, C. Xi, K. Kuroda, Immobilization of amphiphilic polycations by catechol functionality for antimicrobial coatings, Langmuir 27 (7) (2011) 4010–4019, https://doi.org/10.1021/la1046904.